J. Iron Steel Res. Int. (2023) 30:419–428
https://doi.org/10.1007/s42243-022-00824-1

ORIGINAL PAPER

Effects of Na_2CO_3 on reduction mechanism and kinetics of iron during deep reduction of ilmenite concentrate

Xiao-dong Lv[1,2] · You-ling Hou[1,2] · Yun-tao Xin[1,2] · Wei Lv[3] · Xue-wei Lv[1,2]

Received: 1 March 2022 / Revised: 25 April 2022 / Accepted: 26 April 2022 / Published online: 25 August 2022

Abstract

High-quality upgraded titanium slag obtained through semi-molten reduction with the addition of Na_2CO_3 is important for the fluidizing chlorination process to produce TiO_2 pigments. The key is the effect of Na_2CO_3 on the reduction behavior of iron. Therefore, the effects of Na_2CO_3 on reduction mechanism and kinetics of iron during deep reduction of ilmenite concentrate were studied. The results indicated that the metallization ratio of the reduced sample increased with increasing temperature, time, and dose of Na_2CO_3. The addition of Na_2CO_3 significantly accelerated the reduction of iron in the ilmenite concentrate and promoted the growth of iron particles. However, the addition of Na_2CO_3 produced sodium iron titanates; thus, the metallization ratio of the sample decreased with an increase in the temperature and time when the temperature was above 1200 °C and the time was more than 30 min. When the doses of Na_2CO_3 were 0, 3, and 6 wt.%, the reduction of iron was controlled by the interfacial chemical reaction, both the interfacial chemical reaction and diffusion, and diffusion, respectively, and the apparent activation energies were 134.91, 64.89, and 120.82 kJ/mol, respectively.

Keywords Ilmenite concentrate · Sodium carbonate · Metallization ratio · Reduction mechanism · Kinetics

1 Introduction

Titanium metallurgy is a process for extracting titanium and its compounds from titanium minerals. The utilization of low-grade titanium resources has become a mainstream trend with the gradual depletion of high-grade titanium reserves [1, 2]. The current industrial process of smelting low-grade ilmenite is typically operated in an electric furnace facility [3], which is maintained at 1700 °C for 8–10 h. The titanium slag contains 10–12 wt.% FeO, giving it a high fluidity, which is necessary to achieve a high degree of separation of liquid iron from liquid slag. However, the conditions of the aforementioned slagging regime affect the electric furnace smelting process and subsequent processing, as well as the quality and value of the product of titanium slag and pig iron [4–6]. In addition, electric furnace smelting produces considerable pollution, consumes a large amount of energy, and has a low efficiency [7, 8].

One potential process for electric-furnace smelting is solid reduction at a low temperature followed by magnetic separation, because it prevents the inclusion of FeO in titanium slag and reduces energy consumption [9, 10]. However, with this method, the iron particles are too fine, resulting in a low degree of separation of slag and iron [11]. According to previous studies on ilmenite, such as conventional reduction [6, 12, 13], pre-oxidation treatment [5, 14, 15], reduction under vacuum conditions [16–18], and the use of enhanced reduction technologies [19–22], these methods are energy-saving and efficient, and they reduce environmental pollution and improve the grade of the titanium slag. However, owing to the limitations of the equipment, cost, and manufacturers, it is difficult for the new technology to expand production. Therefore, a novel

✉ Yun-tao Xin
xinyuntao0707@163.com

Xue-wei Lv
lvxuewei@163.com

[1] Chongqing Key Laboratory of Vanadium-Titanium Metallurgy and New Materials, Chongqing University, Chongqing 400044, China

[2] College of Materials Science and Engineering, Chongqing University, Chongqing 400044, China

[3] School of Metallurgy, Northeastern University, Shenyang 110819, Liaoning, China

low-energy consumption process that involves Na_2CO_3 addition was proposed for effectively utilizing low-grade ilmenite [23]. In this process, Na_2CO_3 accelerates the reduction and promotes the growth of iron particles. Subsequently, the size of the iron particles satisfies the requirements for a high degree of separation between the slag and iron to produce high-quality titanium slag and pig iron. However, the metallic iron intensifies the reduction mechanism with additive Na_2CO_3 in this process, which needs to be further studied. Lv et al. [20] studied the reduction of iron in the carbothermical reduction of ilmenite concentrate using Na_2SO_4. The results indicated that the metallization ratio decreased as the Na_2SO_4 dose increased. Song et al. [21] examined the effect of $Na_2B_4O_7$ addition on the carbothermic reduction of ilmenite concentrate. With an increase in the $Na_2B_4O_7$ content, the metallization ratio of reduced ilmenite concentrates first increased and then decreased slightly. Huang et al. [24] investigated the reduction of iron during enhancement reduction of ilmenite concentrate with ferrosilicon. It was found that the metallization ratio of iron significantly increased with increases in the Fe–Si amount and reduction time. In addition, El-Tawil et al. [25] investigated the isothermal reduction kinetics of iron in solid-state reduction of ilmenite. The results indicated that apparent activation energies of 251 and 154 kJ/mol were obtained for the phase boundary and diffusion, respectively, in the temperature range of 1000–1200 °C and time range of 0–360 min. Meanwhile, Run et al. [17] researched the non-isothermal reduction kinetics of iron during vacuum carbothermal reduction of ilmenite concentrate with comprehensive consideration of the Šatava–Šesták and Coats–Redfern methods. It was found that an apparent activation energy of 587.4 kJ/mol was achieved for diffusion in the temperature range of 1000–1400 °C.

The objective of the present study was to extend the previous research [23, 26] to study the metallic-iron reduction mechanism and kinetics during the deep carbothermal reduction of ilmenite concentrate by sodium carbonate, according to chemical analysis, Image J analysis, kinetics analysis, and apparent activation energy analysis. These factors were compared systematically under different levels of sodium carbonate addition, which is useful for the selection of the slag–iron magnetic separation in this novel low-energy consumption process involving Na_2CO_3 addition.

2 Experimental

2.1 Materials

The chemical composition of the ilmenite used in this study is presented in Table 1. As shown, the titanium and iron contents were 27.44 and 37.60 wt.%, respectively. The X-ray diffraction (XRD) results for ilmenite are shown in Fig. 1, which indicate that iron exists in the forms of $FeTiO_3$ and Fe_2O_3. The particle size distribution of ilmenite (the reducing agent used) and a schematic diagram of the experimental apparatus have been presented in previous works [23, 26]. The experimental apparatus were a high-temperature silicon–molybdenum furnace with $MoSi_2$ as the heater, as shown in Fig. 2.

2.2 Experimental procedure

Ilmenite concentrate (particle size within the range of 48–150 μm) was the experimental material. Graphite powder (purity $\geq$ 99.9% and grain size $<$ 13 μm) was used as the reducer, and Na_2CO_3 (AR) was used as the additive. According to previous research, the reducer dose was set as 13 wt.%, and the additive dose was set as 0, 3, and 6 wt.% [26]. The experimental temperatures were 1100, 1150, 1200, 1250, 1300, 1350, and 1400 °C, and the reduction time was 5, 10, 20, 30, 60, and 90 min. All materials were dried at 120 °C for 120 min and then were well mixed and pressed into a cylinder with a diameter of 16 mm. When the furnace temperature was increased to the required level, the alumina crucible containing the sample was placed in the furnace quickly, and flowing argon gas (0.6 L/min, purity: 99.99%) was charged in the furnace throughout the reduction process. The reduced sample was quickly removed for water cooling after the heating was finished, and then, chemical analysis was performed to determine the total iron and metallic iron contents. The testing followed the QJ/GY4.003-2007 and QJ/GY4.001-2007 standards. In addition, the samples were analyzed using optical microscopy, scanning electron microscopy (SEM) combined with energy-dispersive X-ray spectroscopy (EDS), and XRD analysis.

The metallization ratio was calculated as follows:

$$\alpha = m_{\mathrm{MFe}}/m_{\mathrm{TFe}} \times 100\%, \quad (1)$$

where α represents the metallization ratio; m_{MFe} represents the mass of metal iron in the reduced sample; and m_{TFe} represents the total iron mass in the reduced sample.

Table 1 Chemical composition of ilmenite concentrate as pure oxides (wt.%)

TiO_2	FeO	Fe_2O_3	SiO_2	MnO	MgO	CaO	V_2O_5	Al_2O_3	P_2O_5	S
45.73	32.41	17.09	2.68	0.78	0.59	0.26	0.198	0.163	0.094	< 0.005

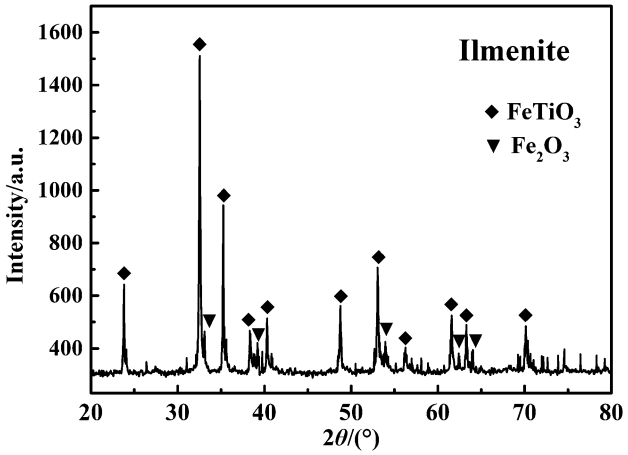

Fig. 1 XRD pattern for ilmenite concentrate. 2θ-Diffraction angle

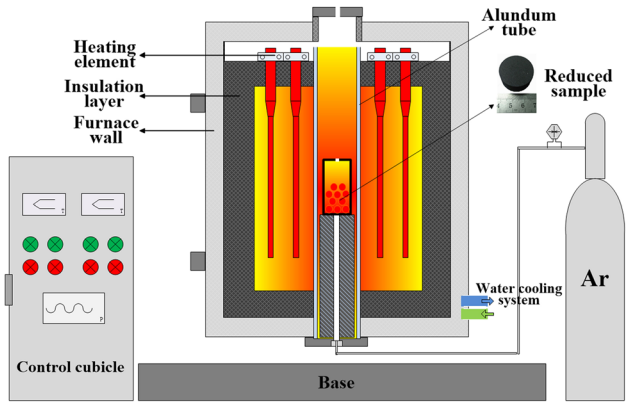

Fig. 2 Schematic of high-temperature silicon–molybdenum furnace

3 Results

3.1 Metallization ratio analysis

Figure 3 shows the metallization ratios of the reduced samples at different reduction temperatures, reduction time, and doses of Na_2CO_3. As shown, the metallization ratio of the reduced sample exhibited similar increasing trends with increases in the reduction temperature and time under different doses of Na_2CO_3. Hence, decreasing the reduction temperature and time can promote iron reduction and enhance its effect. At temperatures above 1200 °C without Na_2CO_3, the change in the metallization ratio mainly occurred within the initial 30 min. Furthermore, the addition of Na_2CO_3 significantly increased the metallization ratio for a given reduction temperature and time. For instance, at reduction temperature of 1100 °C, when the dose of Na_2CO_3 was increased from 0 to 6 wt.% and the reduction time was 20 min, the metallization ratio increased from 26.73% to 65.52%. At a reduction temperature of 1200 °C, the metallization ratio increased from 68.89% to 83.45%. It is speculated that the addition of Na_2CO_3 promoted the reduction of iron in the initial stage of reduction.

However, when Na_2CO_3 was added, the metallization ratio of the sample decreased with increases in the reduction temperature and time when the reduction temperature was above 1200 °C and the reduction time was longer than 30 min. For instance, at a reduction temperature of 1300 °C, when the dose of Na_2CO_3 was increased from 0 to 6 wt.% and the reduction time was 90 min, the metallization ratio decreased from 90.70% to 90.25%. At a reduction temperature of 1400 °C, the metallization ratio decreased from 92.23 to 90.61%. As shown in Fig. 3, the area of the metallization ratio graph exceeding 90% narrowed with an increasing dose of Na_2CO_3. This indicates that a long reduction time was detrimental to the reduction of iron at high temperatures when Na_2CO_3 was added, and the effect became more significant with an increase in the Na_2CO_3 dose, because a small amount of sodium-iron titanates [23] was produced upon Na_2CO_3 addition, resulting in a low metallization ratio.

3.2 Phase transition analysis

As shown in Fig. 1, the main phases of ilmenite are $FeTiO_3$ and Fe_2O_3, and Fe is typically produced by the carbothermal reduction of $FeTiO_3$ and Fe_2O_3. The reduction process of Fe_2O_3 was as follows: $Fe_2O_3 \rightarrow Fe_3O_4 \rightarrow FeO \rightarrow Fe$ [12, 19]. An XRD analysis was performed on the reduced samples treated based on the changes in the metallization ratio of the reduced samples under various reduction conditions to investigate the reduction process of $FeTiO_3$, as shown in Figs. 4, 5, and 6. As shown in Figs. 4 and 5, in the absence of Na_2CO_3, diffraction peaks of $FeTiO_3$, $FeTi_2O_5$, Fe, C, and TiO_2 were observed for the sample at a low temperature of 1100 °C. As the reduction time increased from 5 to 90 min, the diffraction peaks of $FeTiO_3$ gradually weakened and eventually disappeared, and the diffraction peaks of C gradually weakened. The diffraction peaks of $FeTi_2O_5$ disappeared when the reduction time was 90 min.

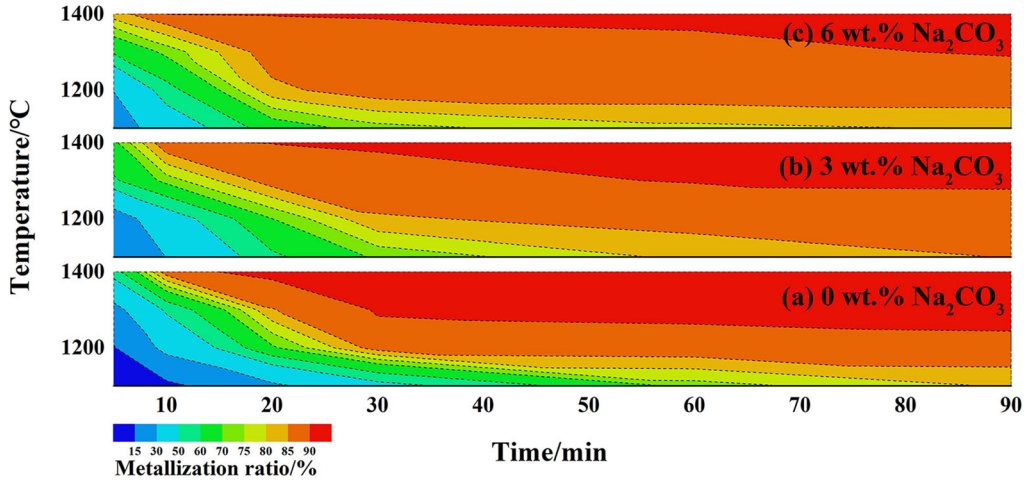

Fig. 3 Contour map of metallization ratio with different reduction temperatures, reduction time, and doses of Na_2CO_3

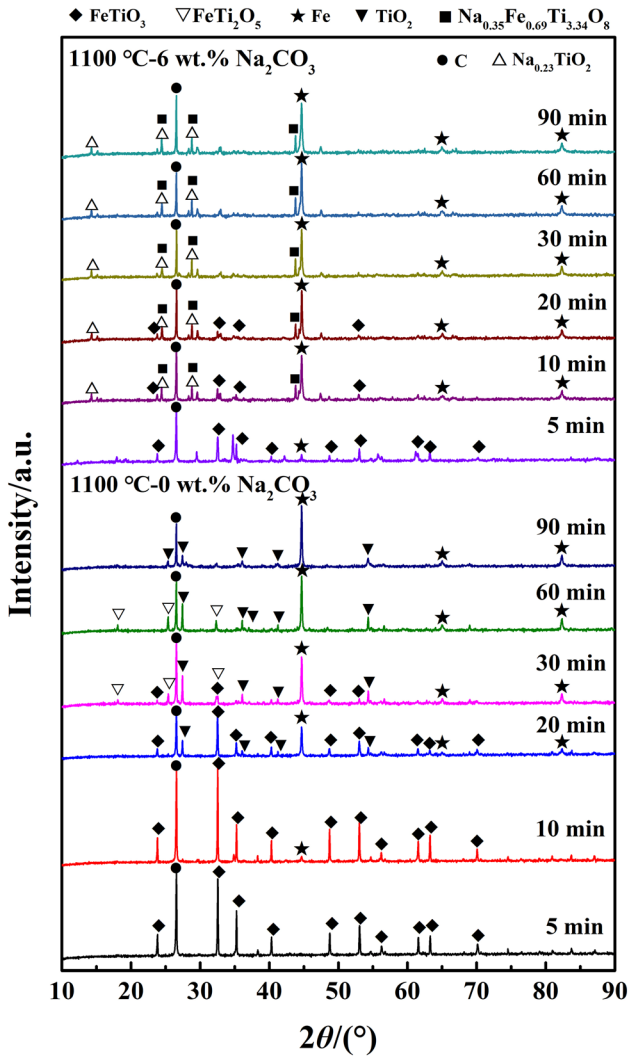

Fig. 4 XRD patterns of samples reduced with different holding time and different doses of Na_2CO_3 at 1100 °C

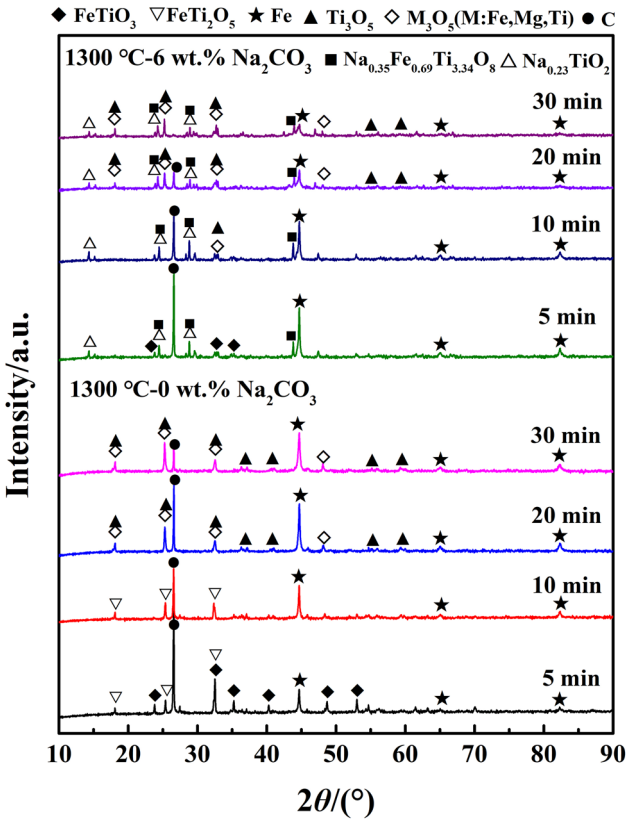

Fig. 5 XRD patterns of samples reduced with different holding time and different doses of Na_2CO_3 at 1300 °C

Therefore, the reduction process of $FeTiO_3$ was as follows: $FeTiO_3 \rightarrow Fe + FeTi_2O_5 + TiO_2 \rightarrow Fe + TiO_2$.However, at a high temperature of 1300 °C, the diffraction peaks of TiO_2 disappeared, and the diffraction peaks of Ti_3O_5 and M_3O_5 (M: Fe, Mg, Ti, etc.) appeared. Therefore, the reduction process of $FeTiO_3$ was changed as follows: $FeTiO_3 \rightarrow Fe + FeTi_2O_5 \rightarrow Fe + Ti_3O_5$. Additionally, as

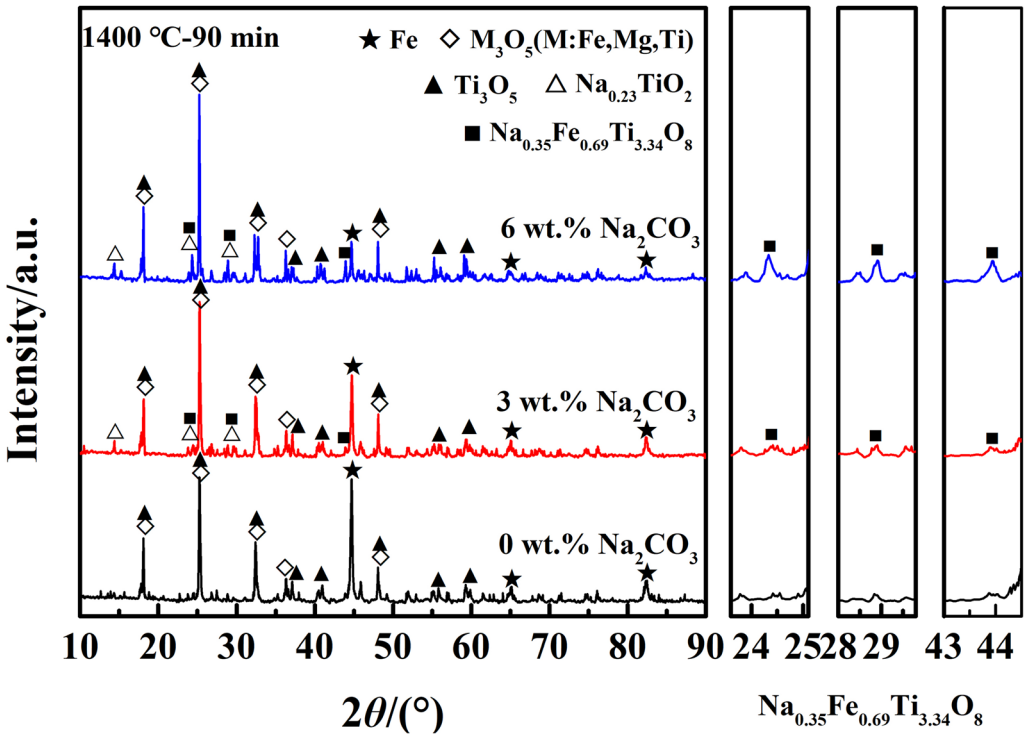

Fig. 6 XRD patterns of samples reduced with different doses of Na_2CO_3, reduction temperature of 1400 °C, and reduction time of 90 min

shown in Figs. 4 and 5, the intensities of the diffraction peaks of Fe increased with the reduction temperature and time. For instance, the intensities of the diffraction peaks of Fe increased suddenly as the reduction time increased from 5 to 20 min at the temperature of 1100 °C. The diffraction peaks of Fe appeared as the reduction temperature increased from 1100 to 1300 °C under the reduction time of 5 min. These results indicated that increases in the reduction temperature and time can accelerate the reduction of iron.

When Na_2CO_3 was added, the diffraction peaks of $FeTiO_3$ weakened and the diffraction peaks of $FeTi_2O_5$ disappeared in the initial reduction stage at 1100 and 1300 °C. These phenomena indicated that the Na_2CO_3 addition significantly promoted the reduction of ilmenite in the preliminary stage. In addition, diffraction peaks of $Na_{0.23}TiO_2$ and $Na_{0.35}Fe_{0.69}Ti_{3.34}O_8$ appeared, and their intensities increased with the Na_2CO_3 dose, as shown in Fig. 6. This is because Na_2CO_3 participated in the reduction of ilmenite to form sodium titanates and sodium iron titanates [23, 27]. The sodium titanates with a low melting point were beneficial to the formation of semi-molten states, which were more conducive to the diffusion, aggregation, and growth of the metal phase [23]. However, as mentioned previously, a small amount of iron oxide easily dissolved into the sodium iron titanates, reducing the metallization ratio of the sample.

3.3 Growth of iron particles analysis

Mineralogical images of the samples reduced at different temperatures and doses of Na_2CO_3 are shown in Fig. 7a. The iron particle size was automatically analyzed using the Image J software. At least six images of different areas were obtained for each sample, and the distribution of the iron particle size and the average size was determined using these images. These parameters are represented by the iron particle diameter in μm, as shown in Fig. 7b.

As shown in Fig. 7, the addition of Na_2CO_3 favored the formation of a semi-molten state, which was more conducive to the diffusion of the solid phase, aggregation, and the growth of the metal phase [23]. For instance, at a reduction temperature of 1400 °C, when the dose of Na_2CO_3 increased from 0 to 6 wt.% and the reduction time was 90 min, the proportion of iron particles with sizes smaller than 48 μm and larger than 75 μm decreased from 82.87% to 17.81% and increased from 1.36% to 66.53%, respectively. Iron particles with sizes above 150 μm were observed when the Na_2CO_3 dose was higher than 6 wt.%. Therefore, the addition of Na_2CO_3 significantly accelerated the growth of iron; with an increasing dose of Na_2CO_3, the average size of the iron particles increased rapidly, and the size of the iron particle distribution region increased. The distribution was concentrated in the region above 13 μm for Na_2CO_3 doses higher than 4 wt.%. Thus, if the Na_2CO_3

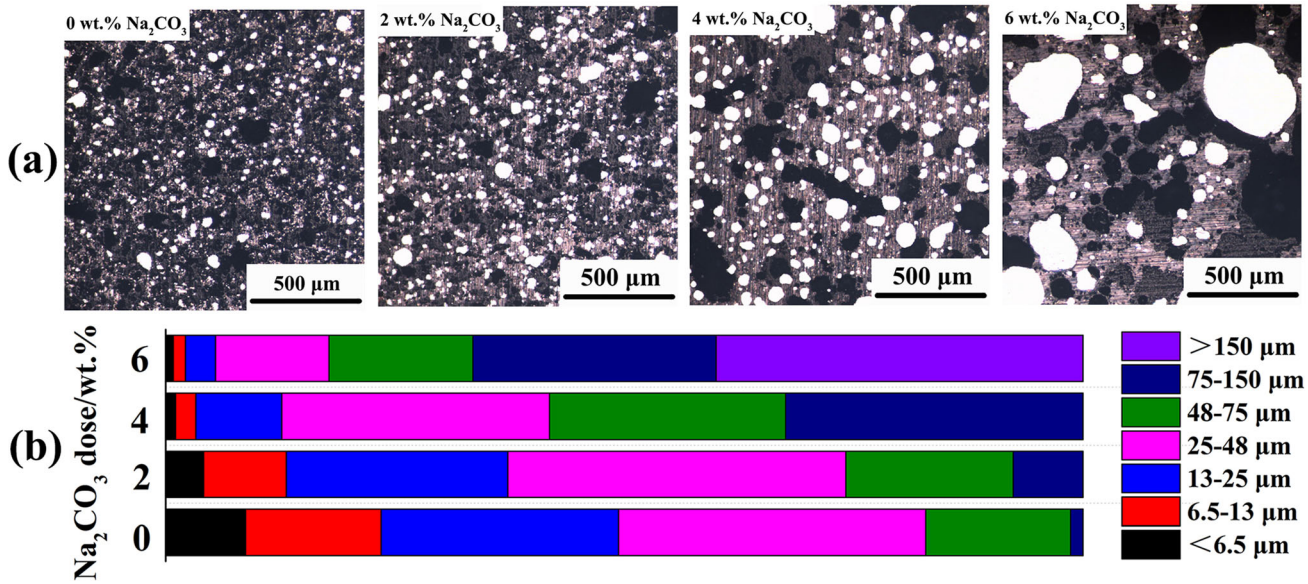

Fig. 7 Mineralogical pictures (**a**) and distribution of iron particle size (**b**) for samples reduced with different doses of Na_2CO_3 at 1400 °C for a holding time of 90 min

dose is further increased, the metallic iron particles will further aggregate and grow.

3.4 Morphology change analysis of iron

The iron particles in the reduced samples were analyzed through SEM and EDS, and the surface area of iron particles was automatically analyzed using the Image J software; the results are shown in Fig. 8. The iron-particle areas mainly consisted of iron, but some areas contained traces of carbon, as indicated by the SEM image of the iron particles and the EDS profile of the areas represented by *a* and *b*. Moreover, there were some dark gray areas in the iron particles, according to the EDS profile of the areas represented by c, d, and e, which can be attributed to oxide inclusion. Various oxides were present in the iron phase while the iron particles grew during the reduction process, which constituted an exogenous inclusion.

4 Discussion

4.1 Kinetics analysis

Generally, the metallization ratio represents the degree of reduction of iron in the reduced sample. As shown in Fig. 3, the change in the metallization ratio mainly occurred within the first 30 min, after which the metallization ratio changed slightly. Moreover, the high temperature accelerated the reaction of iron. At temperatures above 1300 °C, the change in the metallization ratio mainly occurred within the first 10 min when no Na_2CO_3 was added and within the first 5 min when Na_2CO_3 was added. Therefore, only the changes in the metallization ratio that occurred within 30 min during the stage of 1100–1300 °C were considered for the kinetic analysis. Generally, the "mode fit method" is adopted to analyze the kinetics, wherein the experimental data are matched with the kinetics [28, 29]. The metallization ratio under different conditions within 30 min (Fig. 3) was substituted into different kinetic models for the calculation [14, 30]. As shown in Fig. 9, the kinetic control condition with the best fitting degree was selected. As indicated in Fig. 10 and Table 2, the apparent activation energy was determined by fitting the Arrhenius equation [6, 14]. From Table 2, when the doses of Na_2CO_3 were 0, 3, and 6 wt.%, the corresponding kinetic models were expressed by the functions $G(\alpha) = 1 - (1 - \alpha)^{1/3}$, $G(\alpha) = 1 - (1 - \alpha)^{1/3} + [1 - (1 - \alpha)^{1/3}]^2$, and $G(\alpha) = [1 - (1 - \alpha)^{1/3}]^2$, respectively, where $G(\alpha)$ is the integral form of mechanism function. The apparent activation energies (E_a) were 134.91, 64.89, and 120.82 kJ/mol, respectively. As the Na_2CO_3 dose increased, the reduction process of iron gradually changed from being controlled by an interfacial chemical reaction to being controlled by diffusion, and the apparent activation energy first decreased and then increased. This is because a molten phase was produced upon the addition of Na_2CO_3, which promoted the mass transfer [31] and the direct reduction of the ilmenite concentrate [27], reducing the apparent activation energy. However, the molten phase was

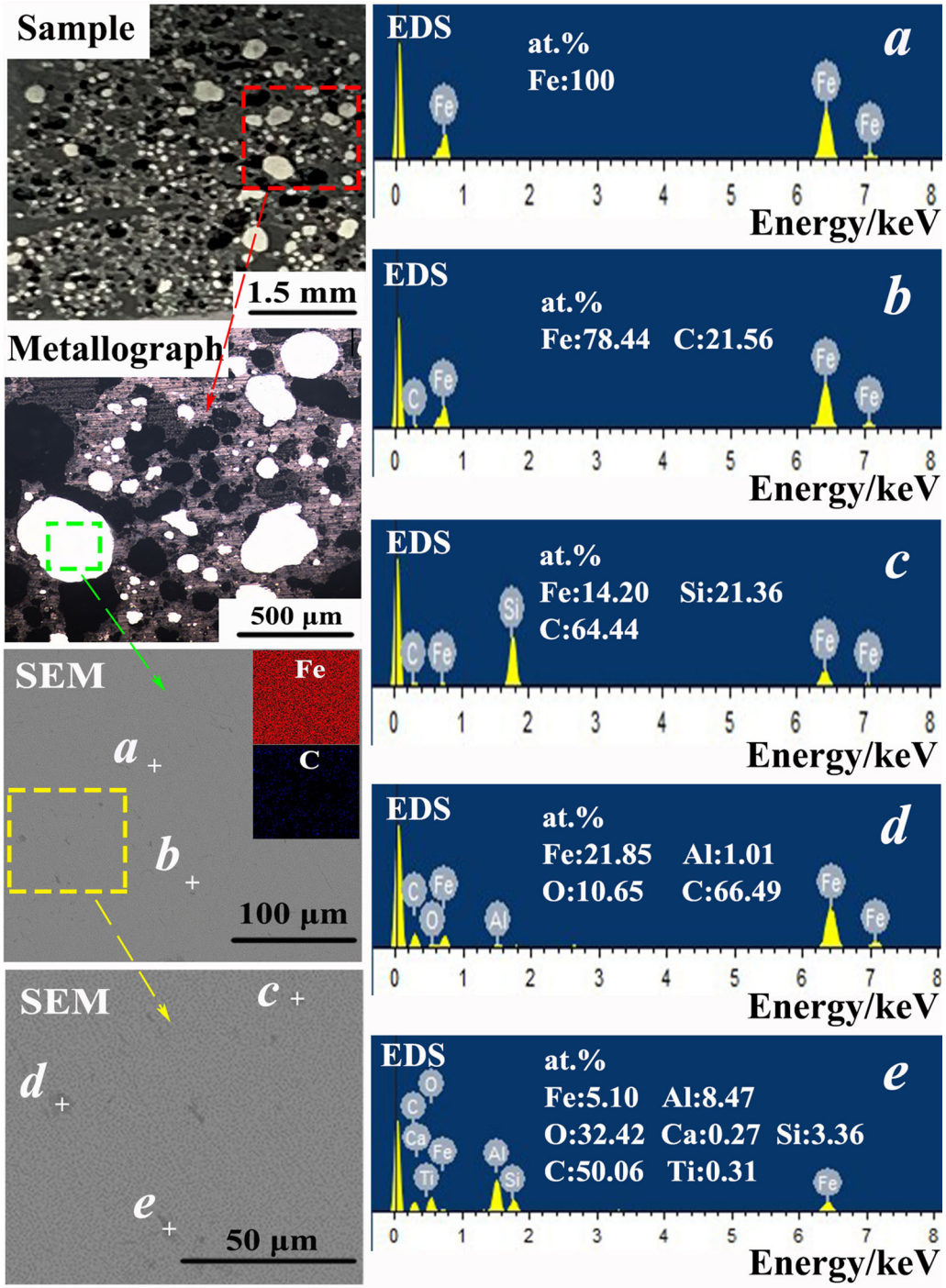

Fig. 8 Morphological changes of iron (carbon content of 13 wt.% and Na_2CO_3 dose of 6 wt.% with a reduction temperature of 1400 °C and reduction time of 90 min. **a**–**e** EDS results for metal iron)

produced, and the amount of molten phase increased as the Na_2CO_3 dose increased to 6 wt.%, which reduced the diffusion rate of the gas during reduction and degraded the condition of the iron reduction reaction [23, 26], resulting in the apparent activation energy increasing again.

4.2 Mechanism analysis

As mentioned previously, Fig. 1 indicates that the iron in the ilmenite mainly existed in the form of $FeTiO_3$. Hence, according to the form of $FeTiO_3$, the metallic iron reduction and growth mechanism during the deep carbothermal

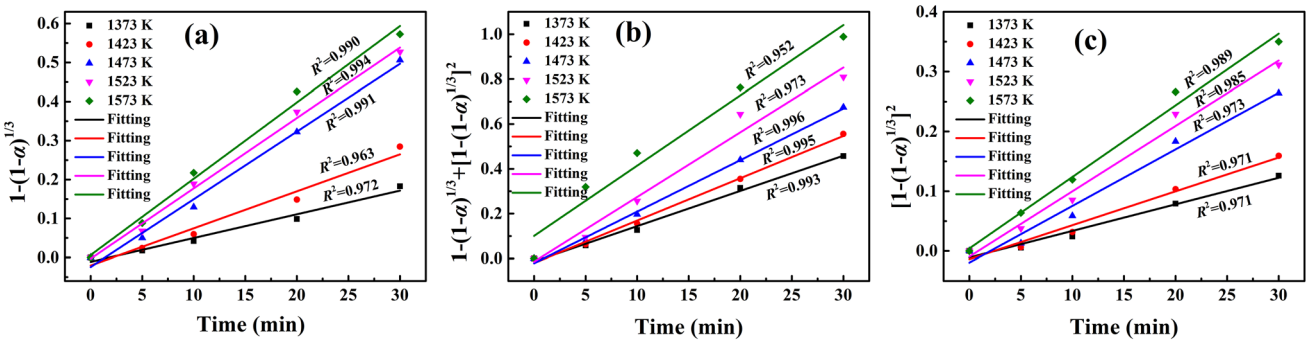

Fig. 9 Relationship between fitting diagrams of mechanism functions and reduction time under different conditions. **a** 0 wt.% Na_2CO_3; **b** 3 wt.% Na_2CO_3; **c** 6 wt.% Na_2CO_3. R^2—Determination coefficient

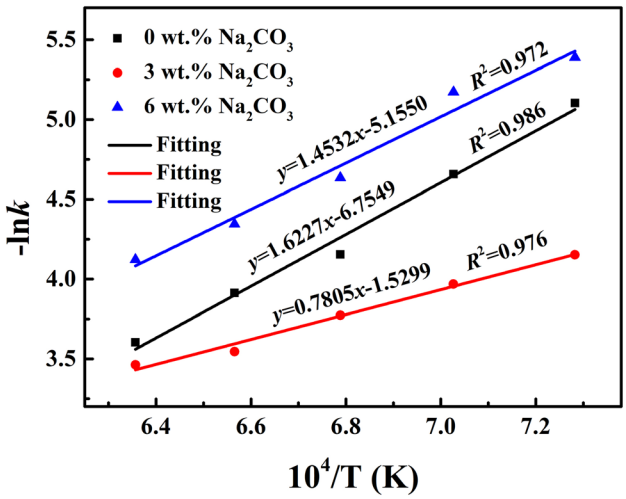

Fig. 10 Relationship between ln(k) and 1/T for different doses of Na_2CO_3. k—Slope obtained by fitting in Fig. 9; T—Kelvin temperature

reduction of ilmenite concentrate by Na_2CO_3 were investigated, as shown in Fig. 11. The initial stage of the reduction reaction is a solid–solid reaction. The carbon in direct contact reacts with the ilmenite concentrate to form a product layer and CO_2. The carbon gasification reaction occurs as the reduction reaction progresses and the temperature increases, and the generated CO replaces the solid carbon and diffuses into the product layer as a reducing agent for the gas–solid reaction. When Na_2CO_3 was added, although the molten phase reduced the gas diffusion capacity and degraded the condition of the reduction reaction, it increased the solid diffusion capacity, which was beneficial to the diffusion-induced migration of iron particles [23, 31]. Additionally, it increased the probability of contact between iron particles, promoting the diffusion, aggregation, and growth of iron particles. Furthermore, the addition of Na_2CO_3 has a catalytic effect on the carbon gasification reaction [32, 33], increasing the reaction rate [27]. Finally, the metallic iron was dispersed in the sample without Na_2CO_3 addition, whereas for the samples with Na_2CO_3 addition, the metal iron aggregated and grew into large particles that are visible to the naked eye, thus ensuring a good separation effect of slag and iron for obtaining high-grade titanium slag and iron concentrate powder. This led to a high efficiency and clean reduction of ilmenite concentrate.

5 Conclusions

1. The metallization ratio of the reduced sample increased with the reduction temperature, reduction time, and dose of Na_2CO_3. The addition of Na_2CO_3 significantly promoted the reduction of iron in the preliminary stage. At reduction temperatures above 1200 °C and reduction time longer than 30 min, the metallization ratio of the sample decreased with increases in the reduction temperature and time. There were traces of oxide inclusions in the iron phase.

Table 2 Control models and kinetic parameters for different doses of Na_2CO_3

Na_2CO_3 dose	Control link	Kinetic model	$G(\alpha)$	E_a/(kJ mol^{-1})
0 wt.%	Interfacial chemical reaction control	Three-dimensional phase boundary reaction	$1-(1-\alpha)^{1/3}=kt$	134.91
3 wt.%	Mixed control of interfacial chemical reaction and diffusion	Three-dimensional phase boundary reaction	$1-(1-\alpha)^{1/3}=kt$	64.89
		Three-dimensional diffusion	$[1-(1-\alpha)^{1/3}]^2=kt$	
6 wt.%	Diffusion control	Three-dimensional diffusion	$[1-(1-\alpha)^{1/3}]^2=kt$	120.82

t—Time

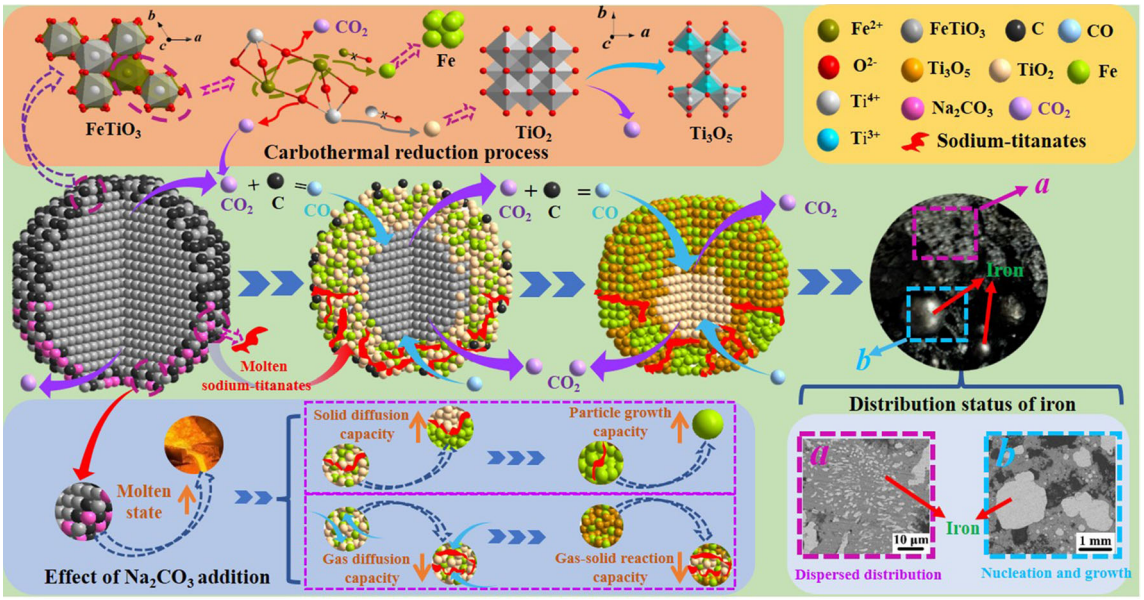

Fig. 11 Mechanism diagram of metallic-iron reduction and growth during deep carbothermal reduction of ilmenite concentrate by Na_2CO_3

2. The initial stage of the reduction reaction was a solid–solid reaction. The carbon gasification reaction occurred as the reduction reaction progressed and the temperature increased, and the generated CO replaced the solid carbon and diffused into the product layer as a reducing agent for the gas–solid reaction. The addition of Na_2CO_3 increased the solid diffusion capacity and the probability of contact between iron particles, which significantly accelerated the growth of iron.
3. When the Na_2CO_3 doses were 0, 3, and 6 wt.%, the reduction of iron was controlled by the interfacial chemical reaction, both the interfacial chemical reaction and diffusion, and diffusion alone, respectively. The corresponding kinetic models were expressed by the functions $G(\alpha) = 1 - (1 - \alpha)^{1/3}$, $G(\alpha) = 1 - (1 - \alpha)^{1/3} + [1 - (1 - \alpha)^{1/3}]^2$, and $G(\alpha) = [1 - (1 - \alpha)^{1/3}]^2$, and the apparent activation energies were 134.91, 64.89, and 120.82 kJ/mol, respectively.

Acknowledgements This work was supported by the National Natural Science Foundation of China (Grant Nos. U1902217 and 52104325). The authors are especially grateful to Pangang Group Research Institute Co., Ltd., China.

Conflict of interest The authors declare that they have no known competing financial interests or personal relationships that could have appeared to influence the work reported in this paper.

References

[1] C.S. Kucukkaragoz, R.H. Eric, Miner. Eng. 19 (2006) 334–337.
[2] R. Huang, X.W. Lv, C.G. Bai, Q.Y. Deng, S.W. Ma, Can. Metall. Quart. 51 (2012) 434–439.
[3] J. Dang, G. Zhang, K. Chou, J. Alloy. Compd. 619 (2015) 443–451.
[4] R. Huang, P. Liu, X. Qian, J. Zhang, Vacuum 134 (2016) 20–24.
[5] H.P. Gou, G.H. Zhang, K.C. Chou, ISIJ Int. 55 (2015) 928–933.
[6] Y. Zhang, W. Lü, X. Lü, S. Li, C. Bai, B. Song, K. Han, Int. J. Miner. Metall. Mater. 24 (2017) 240–248.
[7] N. Ma, N.A. Warner, Can. Metall. Quart. 38 (1999) 165–173.
[8] M. Liu, X. Lv, E. Guo, P. Chen, Q. Yuan, ISIJ Int. 54 (2014) 1749–1754.
[9] C. Geng, T. Sun, H. Yang, Y. Ma, E. Gao, C. Xu, ISIJ Int. 55 (2015) 2543–2549.
[10] Y.F. Guo, H.M. Liu, T. Jiang, C.M. Xiao, G. You, J. Iron Steel Res. Int. 16 (2009) 496–500.
[11] D.S. Chen, B. Song, L.N. Wang, T. Qi, Y. Wang, W.J. Wang, Miner. Eng. 24 (2011) 864–869.
[12] D. Nayak, N. Ray, N. Dash, S.S. Rath, S.K. Biswal, J. Cent. South Univ. 27 (2020) 1678–1690.
[13] H.P. Gou, G.H. Zhang, K.C. Chou, Metall. Mater. Trans. B 46 (2015) 48–56.
[14] W. Lv, X. Lv, Y. Zhang, S. Li, K. Tang, B. Song, Powder Technol. 320 (2017) 239–248.
[15] W. Lv, X. Lv, J. Xiang, J. Wang, X. Lv, C. Bai, B. Song, Int. J. Miner. Process. 169 (2017) 176–184.
[16] X. Lv, R. Huang, Q. Wu, Q. Wu, J. Zhang, Can. Metall. Quart. 58 (2019) 419–426.
[17] H. Run, L. Xiaodong, W. Qinghui, W. Qinzhi, Z. Jinzhu, Metall. Mater. Trans. B 50 (2019) 816–824.
[18] X. Lv, R. Huang, Q. Wu, B. Xu, J. Zhang, Vacuum 160 (2019) 139–145.
[19] N.S. Randhawa, S. Prasad, Metall. Mater. Trans. B 50 (2019) 1277–1289.
[20] W. Lv, C. Bai, X. Lv, K. Hu, X. Lv, J. Xiang, B. Song, Powder Technol. 340 (2018) 354–361.
[21] B. Song, X. Lv, H.H. Miao, K. Han, K. Zhang, R. Huang, ISIJ Int. 56 (2016) 2140–2146.

[22] L. Zhang, X. Guo, Q. Tian, D. Li, S. Zhong, H. Qin, Miner. Eng. 178 (2022) 107403.
[23] X. Lv, Y. Xin, X. Lv, W. Lv, J. Dang, Metall. Mater. Trans. B 52 (2021) 351–362.
[24] R. Huang, X. Lv, C. Bai, K. Zhang, G. Qiu, Steel Res. Int. 84 (2013) 892–899.
[25] S.Z. El-Tawil, I.M. Morsi, A.A. Francis, Can. Metall. Quart. 32 (1993) 281–288.
[26] X. Lv, D. Chen, Y. Xin, W. Lv, J. Dang, X. Lv, Powder Technol. 392 (2021) 14–22.
[27] S.Z. El-Tawil, I.M. Morsi, A. Yehia, A.A. Francis, Can. Metall. Quart. 35 (1996) 31–37.
[28] M.J. Starink, J. Mater. Sci. 42 (2007) 483–489.
[29] S.L. Kharatyan, H.A. Chatilyan, A.S. Mukasyan, D.A. Simonetti, A. Varma, AIChE J. 51 (2005) 261–270.
[30] P. Li, Q. Yu, H. Xie, Q. Qin, K. Wang, Energy Fuels 27 (2013) 4810–4817.
[31] J. Diao, X. Liu, T. Zhang, B. Xie, Int. J. Miner. Metall. Mater. 22 (2015) 249–253.
[32] D.M. McKee, Fuel 62 (1983) 170–175.
[33] B.J. Wood, R.H. Fleming, H. Wise, Fuel 63 (1984) 1600–1603.